



Morphological characteristics and formation mechanisms of the UD-CFRP drill exit-damages

Fei Su^{1,2} · Zhaohui Deng^{1,2} · Xinyi Qiu¹ · Fujian Sun^{1,2} · Qiaoping Wu^{1,2}

Received: 21 June 2019 / Accepted: 6 March 2020 / Published online: 19 March 2020
© Springer-Verlag London Ltd., part of Springer Nature 2020

Abstract

Carbon fiber-reinforced plastic (CFRP) is used widely in many industries. During drilling CFRP, exit drill-induced defects such as burrs and delamination are easy to occur. In the existing model, the crack zone is assumed as a circle or an ellipse, and concrete forming process of the delamination and the burrs does not be truly involved. In this study, the formation mechanisms of the delamination and the burrs are analyzed based on the analytical model and the experimental observation. The results indicate that the critical thrust force only reflects the vulnerability of the crack, but cannot determine the size of the crack. The critical deflection of the fibers tip corresponding to the interlaminar crack extension point determines the size of crack. The burrs appear in four fundamental types.

Keywords Carbon fiber-reinforced plastic (CFRP) · Delamination · Burrs · Drilling

1 Introduction

Carbon fiber-reinforced plastic (CFRP) is applied as substitutions for the metals in lots of weight-critical components in aerospace because of the good properties, such as high specific strength, high specific stiffness, and high modulus [1–5]. In order to obtain desired geometrical shapes and tolerances for a final component, subsequent machining operations are necessary to be required for aircraft manufacturing [6], such as milling and drilling. In fact, drilling is mostly performed as a post-fabrication operation for CFRP parts and components. For example, in order to produce a F-22 aircraft, as many as 14,000 holes need to be drilled [7, 8]. However, drilling of CFRP is still challenging because drilling CFRP is liable to produce serious defects surrounding the hole circumferences

and inside the hole wall surfaces, such as delamination, cracking, fiber pull-out, and burning. In general, exit-delamination is the most critical one because it can critically downgrade the performance of the parts [9].

Upto now, a number of researchers focused their studies on the investigations of these defects to improve the drilling qualities. In accordance with Rahme et al. [10], these defects were directly induced by the drilling thrust force, especially the delamination. In general, the exit drill-induced defects are mainly affected by the thrust force. Generally, if the thrust force exceeds a critical thrust force leading to the onset of delamination, the defects will occur. Then, lots of researchers have modeled to determine the critical thrust force (CTF). Hocheng and Dharan [11] employed the linear elastic fracture mechanics (LEFM), classical plate bending theory, and energy conservation theory to establish an analytical model for calculation of CTF. In their model, a concentrated point load was applied at the center of the plate and the crack zone was assumed as a circle. This is the first analytical model to estimate the CTF. Subsequently, lots of developed models are established based on the same theories. Ismail et al. [12] developed an analytical thermo-mechanical model to estimate CTF. In their model, the crack zone was assumed as an ellipse, and the forces on the chisel edges and the cutting lips were modeled as a concentrated load and a uniformly distributed load, respectively. Saoudi et al. [13] presented a unique analytical model for elliptical delamination zone to estimate CTF.

This is an original paper which has neither previously, nor simultaneously, in whole or in part been submitted anywhere else.

✉ Fei Su
sfeihe@163.com

¹ Hunan Provincial Key Laboratory of High Efficiency and Precision Machining of Difficult-to-Cut Material, Hunan University of Science and Technology, Xiangtan 411201, China

² Intelligent Manufacturing Institute of HNUST, Hunan University of Science and Technology, Xiangtan 411201, China

In their model, the effects of the chisel and the cutting edges were considered. Ojo et al. [14] also developed an analytical model in which the delamination zone was also supposed as an ellipse. They considered the mode I and model II strain energy release rates in delamination zone in their model. Alternatively, Girot et al. [15] proposed an analytical model in which the crack zone was assumed as a circle. They engaged a mixed model strain energy release rate into their model. However, in fact, the crack zone is not truly a circle or an ellipse. In most of the mentioned above models, the crack zone is assumed as a circle or an ellipse. Under this nonrealistic fixed boundary condition, the accurate predictions of the CTF can be affected in the solutions. Kim et al. [16] pointed out that the CTF was overestimated due to this assumption. Furthermore, the concrete forming process of the delamination cannot be truly well-understood according to these models.

As mentioned above, the drill-induced exit delamination has been recognized as the most critical defect, because it can considerably reduce the stiffness and the load carrying capacity of the mechanical parts. Many researchers have focused almost exclusively on the delamination. Actually, the burrs are also the most frequent exit damages during drilling CFRP. The appearance of them may also cause several problems. Then, some additional machining may be engaged to remove the burrs (i.e. deburring), which will increase the cost and time of the production. The expensive CFRP composite parts may be rejected at the last stage of their production cycle [17]. Some researchers have been done to investigate the formation mechanism of the burrs, to search for clarity about how to reduce burrs. A large number of investigations have revealed that the formations of the burrs are strongly dependent on the fiber orientation [18]. For CFRP milling, there are many researchers have found that the fiber orientation has a significant effect on the burrs. Colligan et al. [19, 20] pointed out that the overlapping fibers (i.e., burrs) appeared in two types accompanying with the delamination, such as uncut fibers and long fragments of loose fibers. Hintze et al. [21, 22] presented that the delamination and the fiber overhangs (or burrs) occurred where the fibers were initially cut in a critical cutting angle range. They proposed a model to predict the development of fiber protrusions during the milling CFRP. Subsequently, Zhou et al. [23] confirmed that the fiber tended to be bent instead of being fractured when the actual bending radius was larger than the minimum bending radius, then the burrs occurred in the fiber cutting angle of the range from 90° to 180° . Voss et al. [24] also presented the distributions of the burrs occurrence zones at different fiber orientations by conducted a number of milling experiments. Islam et al. [25] presented a simple and efficient framework (e.g., up-milled and down-milled) for understanding and predicting the occurrence of the burrs at different fiber orientations during milling of CFRP. In general, the drilling process is more complex than

the milling process, and the forming process of the drill-induced burrs may be different. Then, the formation mechanism of the mill-induced burrs cannot be directly adapted to understand the forming process of the drill-induced burrs. In essence, the formation mechanism of the drill-induced burrs has its own characteristics [26].

Considerable existing literatures attempted to establish the analytical model for determining the CTF. However, in most of these above exiting models, the crack zone is assumed as a circle or an ellipse. And more notably, the concrete forming process of the delamination cannot be truly well-understood according to these models. In this study, in order to better understand the mechanism of drill-induced exit-delamination formation, a novel analytical model is established based on the Winkler elastic foundation beam theory and the cohesive zone model. Furthermore, the formation mechanism of the drill-induced burrs is also analyzed.

2 Modeling of the drilling-induced delamination and burrs

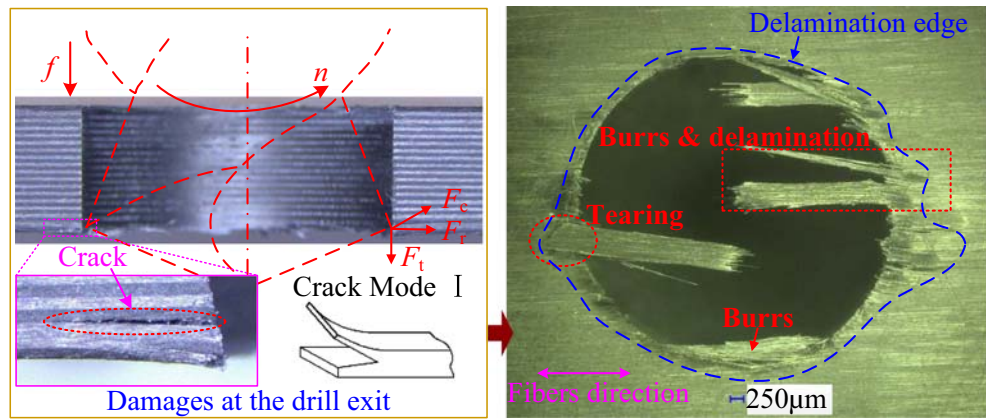
2.1 Formation of the delamination

As mentioned above, the drill-induced defects, such as burrs and delamination, are easy to occur at the hole exit, as shown in Fig. 1. During the drilling of UD-CFRP (unidirectional CFRP), the last ply suffers a thrust force (F_t) and a tangential cutting force (F_c) as well as a radial cutting force (F_r), as illustrated in Fig. 1. Because of this, the surface fibers are bent toward the outside, leading to the occurrences of the delamination as well as the overlapping fibers. In accordance with Jia et al. [17], the extrusions of the main cutting edges are critical to the formation of the final exit delamination and burrs. Among these three components forces, the thrust force is the most critical due to the delamination cracking. Model I is the most prominent damage mechanism because of the low interface bond strength. Furthermore, numerous experimental observations show that the shape and the size of the damages are strongly dependent on the fiber orientation. Andoh et al. [27] and Jin et al. [28] pointed out that the interply delamination zone could be regarded as an elliptical shape during the UD-CFRP drilling. Bao et al. [29] confirmed that the fibers could be removed when the angle between the fiber axis and the cutting direction was an obtuse angle. Conversely, the fibers could not be cut off if this angle was an acute angle, resulting in the overlapping fibers (burrs).

2.2 Exit-ply delamination model for a bunch of fibers

The hole is finished in the cutting stage of the main cutting edges, and the final delamination will be finished mainly by the main cutting edges, during the drilling of CFRP. As

Fig. 1 Formation of the delamination during the drilling of UD-CFRP



mentioned above, a large number of investigations have revealed that the delamination is closely related to the thrust force, and the interlaminar failure occurs once the actual thrust force exceeds the critical thrust force corresponding to the delamination onset. In order to analyze the relationship between the concrete forming process of the delamination and the thrust force and to simplify modeling, the surface material in the exit-delamination zone can be approximately regarded as several semi-infinite elastic ground beams. The section shape of these beams can be regarded as a rectangular [30]. Here, only interlaminar failure is analyzed. Simultaneously, a bilinear cohesive zone model is engaged to depict the interply damage evolutionary law. Additionally, the angle between the axis of the beam and the axis of the warp fibers is defined as θ ($0^\circ \leq \theta \leq 360^\circ$), as described in Fig. 2. In this model, the beam can be approximately regarded as a homogeneous body, but the elastic modulus of the beam at different θ is different owing to the anisotropy of the UD-CFRP, and the equivalent elastic modulus of beam at different θ can be calculated by θ , as shown in Eq. (1) [31].

$$E_{eq} = \left[\frac{1}{E_1} \cos^4 \theta + \left(\frac{1}{G_{12}} - \frac{2\mu_{21}}{E_1} \right) \sin^2 \theta \cos^2 \theta + \frac{1}{E_2} \sin^4 \theta \right]^{-1} \tag{1}$$

According to the experimental observation, most of the fiber overhangs (or burrs) fractured or loosened at their roots, as depicted in Fig. 3. Then, it is assumed that the influence of the thrust force acted on the overlapping fiber on the bending deflection of the whole fiber can be ignored. Accordingly, it is assumed that the fibers are almost flush with the hole edge during the pushing of the main cutting edges. Thus, the maximum bending deflection of the fiber can be regarded as the last feed displacement. The cracking model is illustrated in Fig. 3. The beam is squeezed by the thrust force $p(x)$ during the cutting of the main cutting edge, but the pushing of $p(x)$ is not endless. According to the assumption above and the drilling process, the pushing of $p(x)$ may be terminated because of the feed-stop of the drill bit. As a result, the interlayer delamination can be also automatically terminated because of the feed-stop of the drill bit. The final bending model and the bilinear cohesive zone model are presented in Fig. 3.

In the model, the beam is bent by the pushing of the load $p(x)$. Then, the matrix microcracking or interfacial debonding occurs when the bending deformation of the beam reaches a certain degree. Here, the initial cracking length of the beam is defined as a_0 . According to Liu et al. [32, 33], the relationship between the traction t and the crack opening displacement Δ can be written by Eq. (2).

$$t = (1-D)K\Delta \tag{2}$$

Where

$$D = \begin{cases} 0 & (\Delta \leq \Delta_0) \\ \frac{\Delta_f(\Delta - \Delta_0)}{\Delta(\Delta_f - \Delta_0)} & (\Delta_0 < \Delta < \Delta_f) \\ 1 & (\Delta_f \leq \Delta) \end{cases} \tag{3}$$

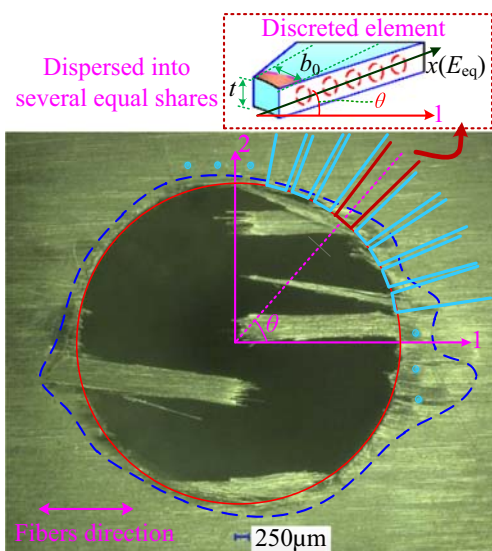


Fig. 2 Definition of θ (angle between the axis of each beam and the axis of the warp fibers)

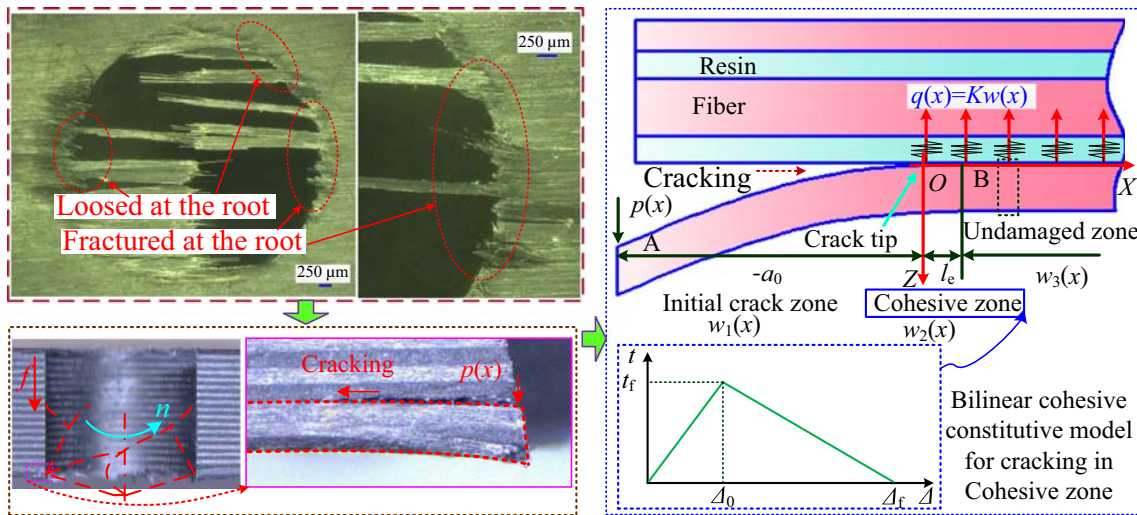


Fig. 3 Discretization model of the exit-ply [33]

K, D, Δ_0 , and Δ_f are the interfacial foundation stiffness, the damage parameter, the displacement for damage initiation, and the displacement for damage completion [32, 33].

The model I critical fracture energy release rate G_{IC} and the interface tensile strength t_f can be determined by [32, 33].

$$\begin{cases} G_{IC} = 2t_f \Delta_f \\ t_f = K \Delta_0 \end{cases} \quad (4)$$

Lachaud et al. [34] reported that the model I critical fracture energy release rate G_{IC} can be determined by the angle between two plies. The angle between the beam axis and the fiber axis can be defined as φ . Then, the fracture energy release rate G_{IC} at different θ can be introduced by curve fitting method according to the test data from Lachaud et al. [34], as the following

$$G_{IC} = 0.01481\varphi^2 + 0.2222\varphi + 120 \quad (5)$$

Where

$$\varphi = \begin{cases} \theta & (0^\circ \leq \theta \leq 90^\circ) \\ 180 - \theta & (90^\circ < \theta \leq 180^\circ) \\ \theta - 180 & (180^\circ < \theta \leq 270^\circ) \\ 360 - \theta & (270^\circ < \theta \leq 360^\circ) \end{cases}$$

In fact, the cracking model of the beam can be divided into two zones, such as the initial crack zone and the undamaged zone. However, there are three zones once the interface damage begins, as illustrated in Fig. 3. These three zones are the initial crack zone (AO), the cohesive zone (OB), and the undamaged zone (BX), respectively. Here, the point O is the crack tip. Therefore, the cracking model can be considered in two stages, namely, before and after the interface damage begins. To solve the final bending models of these two stages, the following three differential equations for each zone can be

expressed by Eq. (6) [33]. Then, the general solutions can be given by Eq. (7) [33].

$$\begin{cases} \frac{d^4 w_1(x)}{dx^4} = 0 & (-a_0 \leq x \leq 0) \\ \frac{d^4 w_2(x)}{dx^4} - \lambda_1^4 w_2(x) + p'_0 = 0 & (0 \leq x \leq l_e) \\ \frac{d^4 w_3(x)}{dx^4} + 4\lambda_2^4 w_3(x) = 0 & (l_e \leq x) \end{cases} \quad (6)$$

$$\begin{cases} w_1(x) = C_1 x^3 + C_2 x^2 + C_3 x + C_4 & (-a_0 \leq x \leq 0) \\ w_2(x) = C_5 \cos(\lambda_1 x) + C_6 \sin(\lambda_1 x) + C_7 e^{\lambda_1 x} + C_8 e^{-\lambda_1 x} + \Delta_f & (0 \leq x \leq l_e) \\ w_3(x) = e^{-\lambda_2 x} (C_9 \cos(\lambda_2 x) + C_{10} \sin(\lambda_2 x)) \\ \quad + e^{-\lambda_2 x} (C_{11} \cos(\lambda_2 x) + C_{12} \sin(\lambda_2 x)) & (l_e \leq x) \end{cases} \quad (7)$$

Finally, the coefficients $C_1 \sim C_{12}$ in Eq. (7) can be obtained by combining the Eq. (7) and the boundary conditions for the system of the differential equations (as given as Eq. (8)) [33].

$$\begin{cases} w_1''(-a_0) = 0, w_1'''(-a_0) = \frac{P}{E_{eq} I_f}, w_3''(\infty) = 0, w_3'''(\infty) = 0 \\ w_1(0) = w_2(0), w_2(l_e) = w_3(l_e), w_1'(0) = w_2'(0), w_2'(l_e) = w_3'(l_e) \\ w_1''(0) = w_2''(0), w_2''(l_e) = w_3''(l_e), w_1'''(0) = w_2'''(0), w_2'''(l_e) = w_3'''(l_e) \end{cases} \quad (8)$$

Where

$$\begin{cases} \lambda_1^4 = \frac{\Delta_0}{\Delta_f - \Delta_0} \frac{b_0 K}{E_{eq} I_f} \\ 4\lambda_2^4 = \frac{b_0 K}{E_{eq} I_f} \\ p'_0 = \frac{\Delta_0}{\Delta_f - \Delta_0} \frac{b_0 K \Delta_f}{E_{eq} I_f} \end{cases} \quad (9)$$

b_0 is the width of the beam. It is equal to the width of the main cutting edge because the width of the contact area is

determined by the main cutting edge. I_f is the moment inertia of the beam.

3 Experimental verification

3.1 Experimental details

A series of drilling tests were carried out on KVC1050M vertical machining center without coolant, by the twist drill bit made of YG6X carbide without coating, with a diameter 6 mm. The drilling parameters with the spindle speed of 2000–5000 rpm (i.e., 2000, 3000, 4000, 5000 rpm) and the feed speed of 105–420 mm/min (i.e., 105, 210, 315, 420 mm/min) were selected. The thrust forces were measured by the dynamometric system. The dynamometric system is composed of a Kistler force sensor (9253B23 dynamometer), a Kistler 5080 amplifier, a PCIM-DAS1602/16 data acquisition as well as a PC. All the experimental setups and the force measurement systems were depicted in Fig. 4.

Unidirectional CFRP laminates (T300/Epoxy) with the thickness of 10 mm and the average thickness per layer of 0.13 mm were used in the tests. The fiber volume content and the average diameter of carbon fibers were $60 \pm 5\%$ and $7\text{--}8 \mu\text{m}$, respectively. The other material properties were listed in Table 1.

In addition, to verify the critical thrust forces at different φ , in accordance with Zitoun et al. [10, 35], some quasi-static punching tests were carried out. Before the punching tests, several pilot holes need to be drill with the reserved thickness about 0.13–0.15 mm (using the twist drill bit with a diameter 6 mm), to ensure the last exit-ply without being cut, as illustrated in Fig. 5a. During the punching tests, the angle between the main cutting edge and the fiber orientation was fixed at a certain degree (typical values: 0° , 30° , 60° , and 90°), as depicted in Fig. 5b. Then, the punching tests were performed by the same twist drill bit at the rate of 1 mm/min, and each test was repeated three times. The critical thrust force of the crack propagation can be decided by the punching thrust

Table 1 Material properties used for model predictions

Items	Value
Longitudinal Young's modulus of fiber E_1	122.6 GPa
Transverse Young's modulus of fiber E_2	7.7 GPa
Shear modulus G_{12}	2.8 GPa
Poisson's ratio $\mu_{12/21}$	0.3
Interface stiffness k	0.47 Pa/mm
Tensile strength of the interface t_f	20 MPa

force. In actual drilling process, the drilling thrust force may be generally larger than the critical thrust force. However, the drilling thrust force values when the main cutting edges of the drill bit drilled the last ply are accurately obtained. Then, here, the punching thrust force value when the main cutting edges of the drill bit drilled the last ply is considered approximately equal to the drilling thrust force. Additionally, the punching thrust force of each main cutting edge is regarded as approximately equal, because the two flutes main cutting edges of the drill bit are symmetrical. Therefore, the average normal load (or average thrust force) of a single edge acted on the last ply can be determined by Eq. (10).

$$P_m = F_t/2t_1 \quad (10)$$

3.2 Damages measurement and quantification

In order to obtain the comprehensive and accurate hole qualities, the one-dimensional delamination factor K_D and two-dimensional delamination factor K_A were provided to characterize exit-delamination level. The delamination factor (K_D) was the ratio of maximum diameter of the damage zone D_{\max} to the hole diameter D_0 , and the delamination factor (K_A) was defined as the ratio between the total area of the drilled hole and delamination (A_d) and the nominal hole area (A_n), as described in Fig. 6. The exit-defects shape and size were measured and were analyzed by KEYENCEVHX-

Fig. 4 Experimental setups

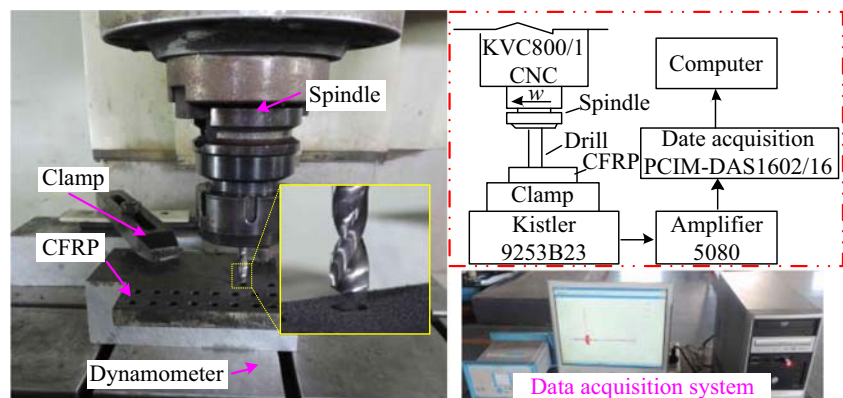
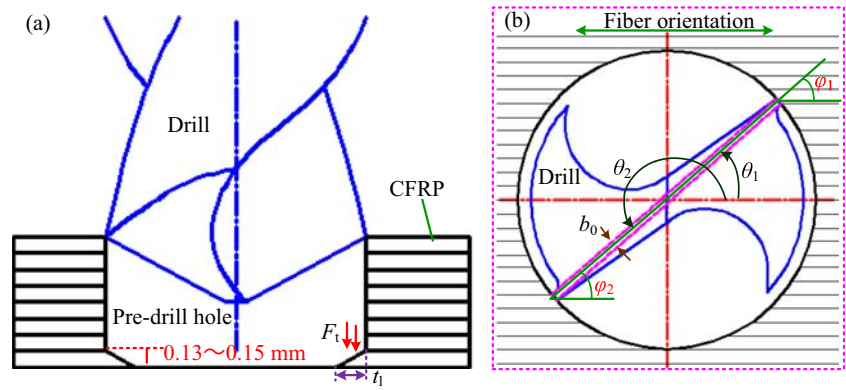


Fig. 5 Quasi-static punching test schemes



500FE digital microscope system as well as its measurement software. The digital microscope system was illustrated in Fig. 6.

Additionally, to analyze the appearance regulation for delamination, a shape factor K_S was introduced [36], as depicted in Eq. (11). As for the definition of K_S , the range of K_S is from 0 to 1. If the shape of the delamination (including tearing) is entirely a circular ring, the value of K_S is equal to 1, and a larger K_S corresponds to a more uniformly distributed delamination; the shape of the delamination is closer to a circle.

$$K_S = \frac{\sqrt{K_A}}{K_D} \tag{11}$$

4 Results and discussion

4.1 Critical thrust force validation

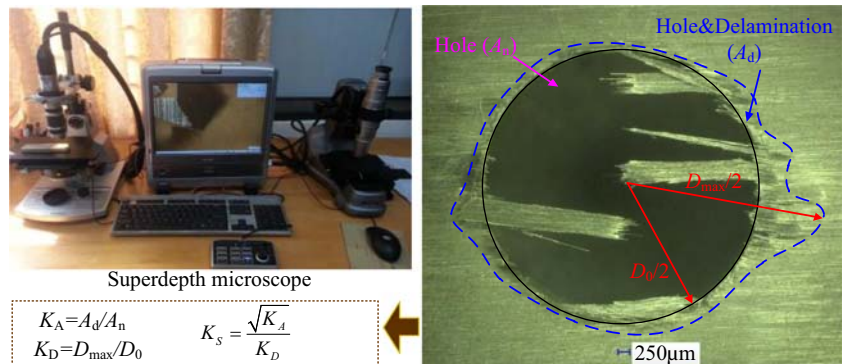
The proposed analytical model for the critical force of the last ply under the pushing by a single main cutting edge is validated experimentally by the punching test. The thrust forces at $\varphi = 0^\circ$, $\varphi = 30^\circ$, $\varphi = 60^\circ$, and $\varphi = 90^\circ$ are obtained, respectively. The total thrust force is produced by the part edges within t_1 during the punching of the last ply, and then the average normal load (or average thrust force) of a single edge acted on the

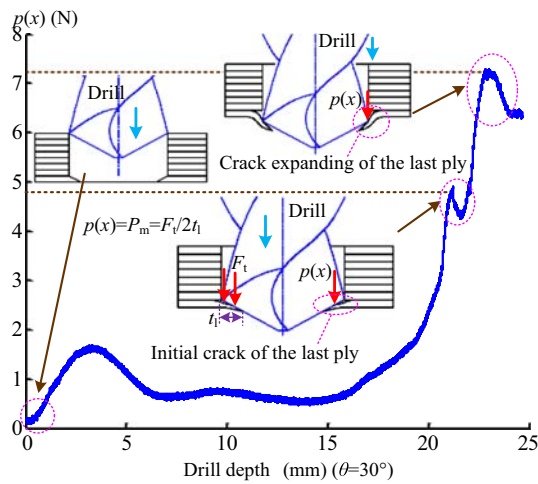
last ply can be obtained. A typical curve of this average normal load is illustrated in Fig. 7a.

In Fig. 7a, the average thrust force is not equal to zero at the beginning owing to the friction between the drill and the hole wall because of the shrinkage of the CFRP hole. The average thrust force begins to increase once the main cutting edges contact with the last ply. Consequently, there are two drops suddenly. During the punching, the two main cutting edges first contact with the last ply, and then the whole of the main cutting edges and the major flanks contact with the last ply.

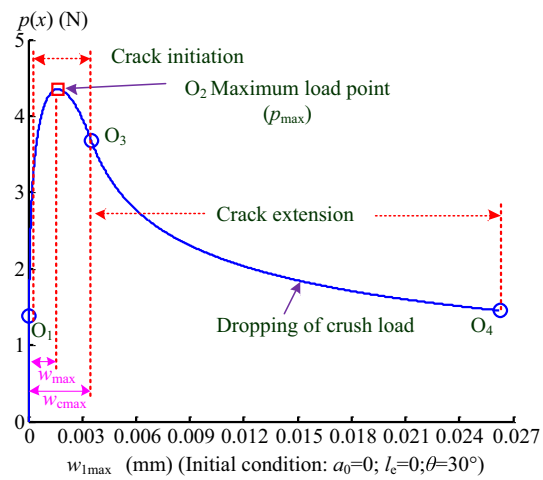
Therefore infers from this, the first drop of the average thrust force mainly due to the interlaminar failure occurs because of the first squeeze of the main cutting edges, and the second drop mainly due to the recurrence of the interlaminar failure induced by the whole of the main cutting edges and the major flanks. The contact surface of the whole of the main cutting edges and the major flanks are obviously greater than that of the main cutting edges; this is a major reason for the higher peak of the second drop. During the cutting of the main cutting edges, the last ply is mainly squeezed by the main cutting edges and almost without the pushing effect of the major flanks on the last ply. The thrust force acted on the last ply is mainly produced by the main cutting edges. Therefore, the average critical thrust force at the onset of the delamination for a single main cutting edge corresponds to the peak of the first drop. Then, these average critical thrust forces when $\varphi = 0^\circ$, $\varphi = 30^\circ$, $\varphi = 60^\circ$, and $\varphi = 90^\circ$ are about 7.72N, 4.85N,

Fig. 6 Evaluation factors





(a) Average normal load (or thrust force) curve



(b) Load-crack opening displacement of beam

Fig. 7 Average thrust force and load-crack opening displacement

4.16N, and 4.42N, respectively. Obviously, these average critical thrust forces vary regularly as φ changes and reach their maximum value when $\varphi = 0^\circ$.

The width of the main cutting edge is around 2 mm, then $b_0 = 2$ mm. Here, the maximum deflection of the beam is set to about 0.026 mm. Figure 7b (initial conditions: $a_0 = 0$, $l_c = 0$ and $\varphi = 30^\circ$) shows the load-crack opening displacement of the beam. The point O_1 , O_2 , O_3 , and O_4 are the elastic deformation limit point, the thrust force peak point, the interlaminar crack extension point, and the pushing termination point, respectively. At the point O_1 , the maximum deflection of the beam (or the deflection of the beam tip, $w_1(x)_{max}$) is equal to the displacement for damage initiation Δ_0 . At the point O_3 , $w_1(x)_{max}$ is equal to the displacement for damage completion, and at the point O_4 , $w_1(x)_{max}$ is equal to 0.026 mm. The evolutive process of the crack can be divided into three stages, viz., elastic deformation ($0 \rightarrow O_1$), crack initiation ($O_1 \rightarrow O_3$), and crack extension ($O_3 \rightarrow O_4$). The elastic deformation process occurs in a very short period of time. In the crack initiation ($O_1 \rightarrow O_3$) period, the interlaminar crack begins, and the thrust force increases to the peak point O_2 then decreases. In the crack extension period ($O_3 \rightarrow O_4$), the interface is fractured and the crack enlarges with increasing the maximum deflection of the beam (or the deflection of the beam tip, $w_1(x)_{max}$), but the thrust force continues to drop. Obviously, the thrust force continues to fall once $w_1(x)_{max}$ exceed the deflection corresponding to the peak point (O_2) (w_{max}), implying that the interlaminar crack is easier to occur. Thus, the point O_2 can be considered as a key point for the initiation and extension of the interlaminar crack, and the thrust force corresponding to this point can be regarded as the critical thrust force at delamination. According to this model, the critical thrust forces when $\varphi = 0^\circ$, $\varphi = 30^\circ$, $\varphi = 60^\circ$, and $\varphi = 90^\circ$ can be estimated at about 7.03N, 4.35N, 3.97N, and 4.28N, respectively. These values and their variation revealed from

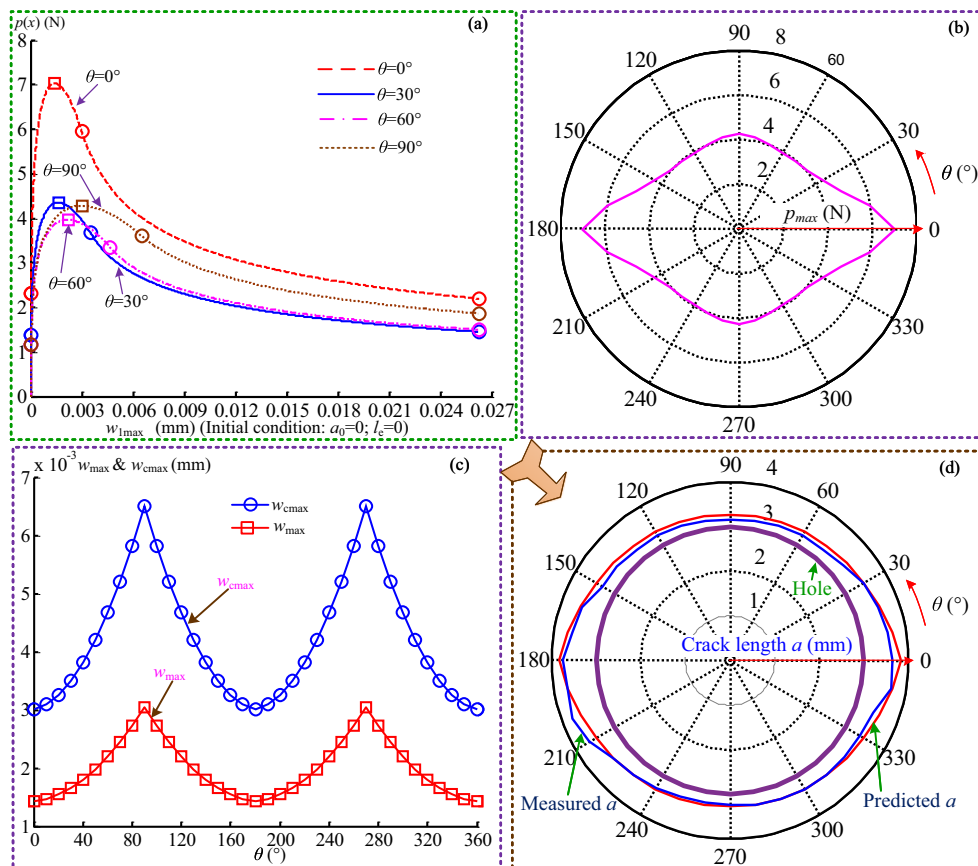
these values are agree with the experimental results, but these values are all less than the experimental values owing to the friction between the drill and the hole wall because of the shrinkage of the CFRP hole.

4.2 Correlation between critical thrust force and delamination

The variation of the critical thrust forces with θ is illustrated in Fig. 8a and b. As shown here, the critical thrust force reach the maximum when $\theta = 0^\circ/180^\circ$, and reach the second largest value when $\theta = 90^\circ/270^\circ$. When θ is around 60° or 240° , the critical thrust force can be minimized. Theoretically, the risk of the delamination can be reduced if the critical thrust force is large; in other words, the final delamination during the drilling will be smaller owing to the higher critical thrust force. Namely, the delamination when $\theta = 0^\circ/180^\circ$ should be minimal and that when θ is around 60° or 240° , should be maximum. However, the facts suggest otherwise. The delamination reaches the maximum exactly when $\theta = 0^\circ/180^\circ$, and attains minimum when $\theta = 90^\circ/270^\circ$, as depicted in Fig. 8d.

In theory, the deflection of the beam tip (namely, the maximum deflection of the beam, $w_1(x)_{max}$) determines the thrust force acted on the beam. As for macro-process, the interlaminar crack occurs once the deflection of the beam tip ($w_1(x)_{max}$) exceeds a certain limit. Additionally, in fact, the deflection of the beam tip ($w_1(x)_{max}$) is a controllable factor. Therefore, the deflection of the beam tip ($w_1(x)_{max}$) is of great significance to controlling the interlaminar crack. As presented in Fig. 7b, w_{max} and w_{cmax} are the deflection of the beam tip corresponding to the peak point (O_2) and that corresponding to the interlaminar crack extension point (O_3), respectively, and w_{cmax} is the critical value for interlaminar crack extension. The variations of w_{max} and w_{cmax} with θ are depicted in Fig.

Fig. 8 Relationship among θ , CTF, w_{\max} , and w_{cmax}



8c. Both w_{\max} and w_{cmax} reach their minimum when $\theta = 0^\circ/180^\circ$ and reach their maximum when $\theta = 90^\circ/270^\circ$.

The displacements of the exit last ply materials at different θ , caused by the pushing of the drill, are basically the same during the drilling. That is, the deflections of the beam tip at different θ are equal basically to each other under the same circumstances. As a result, the sizes of the cracks at different θ are different due to the different critical values for interlaminar crack extension.

If the w_{cmax} value is lower, the crack occurs more rapidly and the size of the crack may be larger. Rather, the crack occurs more slowly and the size of the crack may be smaller. Obviously, the shape and the size of the delamination strongly depend on the variation of the w_{cmax} values. Therefore, the delaminations reach the maximum when $\theta = 0^\circ/180^\circ$ owing to the smallest w_{\max} and w_{cmax} , and reach the minimum when $\theta = 90^\circ/270^\circ$ because of the largest w_{\max} and w_{cmax} .

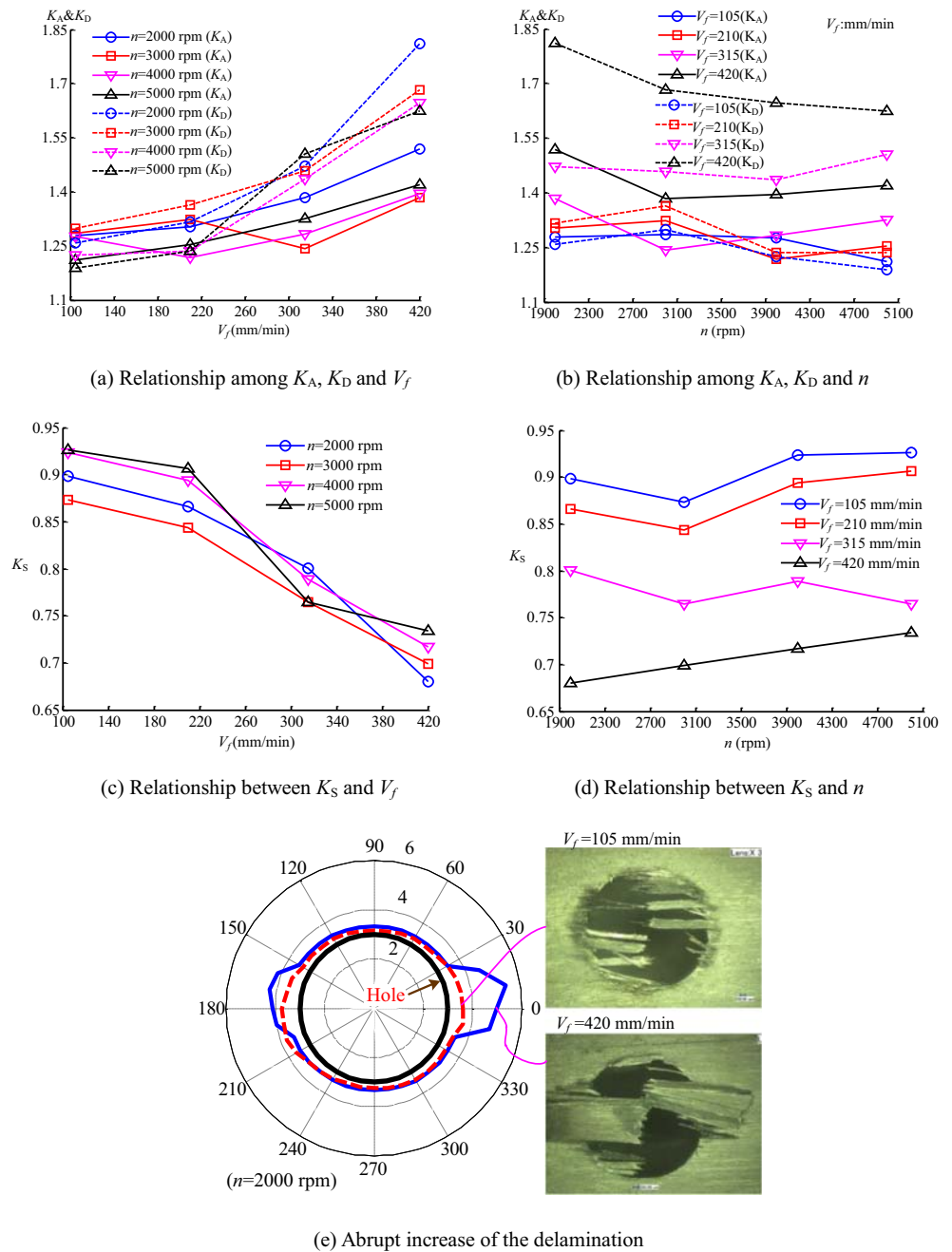
Above knowable, the critical thrust forces may be different and the w_{cmax} values may be also different for different θ . The critical thrust force simply reflects the vulnerability of the crack, but cannot determine the size of the crack. If the critical thrust force is larger, the crack occurs easier. However, what determines the size of the delamination is the w_{cmax} value. Under the same drilling parameters, if the w_{cmax} value is larger, the size of the crack may be

smaller, viz., the size of the delamination may be smaller. In addition, at the same θ , if the deflection of the beam tip ($w_1(x)_{\max}$) is larger, the size of the crack (or delamination) may be larger. In general, the deflection of the beam tip ($w_1(x)_{\max}$) directly relates to the feed rate and the drilling depth. Thus, the feed rate and the drilling depth directly affect the size of the delamination. Actually, in order to control the delamination, the most straightforward and effective method is to control the axial displacement of the last ply materials. For example, drilling with the back-up support can restrain the deflection of the materials at the hole exit [17]. However, the w_{cmax} critical values at different θ are very small, and their order of magnitude is only 10^{-3} mm. In actual processing, it is difficult to keep the w_{cmax} value in this range.

4.3 Exit-delamination shape characteristic

The variations of K_A , K_D , and K_S with V_f and n are presented in Fig. 9a–d. The delamination factors (i.e., K_A and K_D) increase with the increasing feed speed, in other words, both the maximum diameter of the damage zone and the area of the damage zone increase with the increasing feed speed. The delamination factors (i.e., K_A and K_D) decrease with the increasing spindle speed, but their

Fig. 9 Change rules of delamination factors and shape factor



decreasing trends are not obvious, especially the decreasing trend of K_A . Therefore, in contrast, the delamination is more influenced by the feed speed.

The shape factor K_S decreases with the increasing of feed speed, implying that the delamination presents obvious inhomogeneity, and the effect of the fiber orientation on the delamination is more obvious. Here, the shape factor K_S lies in between 0.87 and 0.93; when $V_f = 105$ mm/min, the geometrical shape of the delamination appears approximate a circle or an ellipse, as shown in Fig. 9e. When $V_f = 420$ mm/min, the shape factor K_S drop to 0.68–0.73, and the difference of the lengths between

the major axis and the minor axis is even greater, and the delamination suddenly increases in local region. Observational evidence to confirm that the abrupt increase of the delamination is mainly caused by the tearing when $\theta = 0^\circ/180^\circ$, as presented in Fig. 9e. Although the shape factor K_S increases with the increasing spindle speed when $V_f = 420$ mm/min, generally, the effect of the spindle speed on the shape factor K_S is not obvious. When $V_f = 420$ mm/min, the shape factor K_S ranges from 0.68 to 0.73. Obviously, the influence of the fiber orientation on the delamination cannot be corrected with the increasing spindle speed.

4.4 Exit-burrs shape characteristic

As mentioned above, there is a strong correlation between the burrs formation and the cutting condition. For example, the burrs do not occur when the angle between the fiber axis and the cutting direction is an obtuse angle, rather, the burrs may occur as this angle is an acute angle [26, 29]. Considering the cutting process of the last ply materials during the drilling of the main cutting edges, the thickness of the uncut materials is defined as t_1 when the main cutting edges cut the last ply materials. The cutting state of the fibers may be changed regularly with the drill rotation. According to analysis, the cutting state can be classified into four cases when the drill is rotated a half-turn from the point I, as illustrated in Fig. 10a.

1) From the point I to the point J, the fibers may be difficult to be cut off at the point I due to the angle between the fiber axis and the cutting direction is less than 90 degrees, then the uncut fibers may be pushed toward the hole exit by the main cutting edges. The angle between the fiber axis and the cutting direction is greater than 90 degrees when the drill continues to be rotated, but the fibers still cannot be removed owing to the uncut fibers continue to be bent and evade the cutting edge, because the uncut fibers have been bent or torn toward the hole exit. Then, the whole uncut fibers may be stripped away, as illustrated in the cutting model of the region P_1 (in Fig. 10a). Therefore, the final burrs are much more likely to occur in this region, especially when the thickness

- of the uncut materials t_1 is so small. The uncut fibers may be easier to be peeled up owing to the weak interlayer bond when t_1 is small.
- 2) In region P_2 , the contact point between the fibers and the main cutting edges is located in the rake face due to the angle between the fiber axis and the cutting direction is too large. The fibers may be peeled up and compressed, inducing the interlaminar crack in fiber direction and the axial buckling as well as the fiber bundles failure due to exceeding the flexural strength. Then, saw teeth topography is mapped on the edge of hole due to the final breakpoints which are below the cutting surface [37]. Therefore, there are no burrs in this region.
 - 3) In region P_3 , the contact point between the fibers and the main cutting edges moves toward the nose of the main cutting edge because the angle between the fiber axis and the cutting direction reduces gradually. Then, the fibers may not be compressed, but may be bent. By then, the fibers may well evade the cutting edge by this bending, resulting into the burrs. In the meanwhile, the interlaminar crack may be induced due to the fibers are peeled up.
 - 4) In region P_4 , the angle between the fiber axis and the cutting direction is less than 90 degrees, and the contact point between the fibers and the main cutting edges is located at the nose of the main cutting edge. The fibers are easy to be bent and evade the cutting edge. Then, the burrs are prone to occur owing to this avoidance behavior. Meanwhile, interlaminar crack is also prone to occur due to the fibers are peeled up.

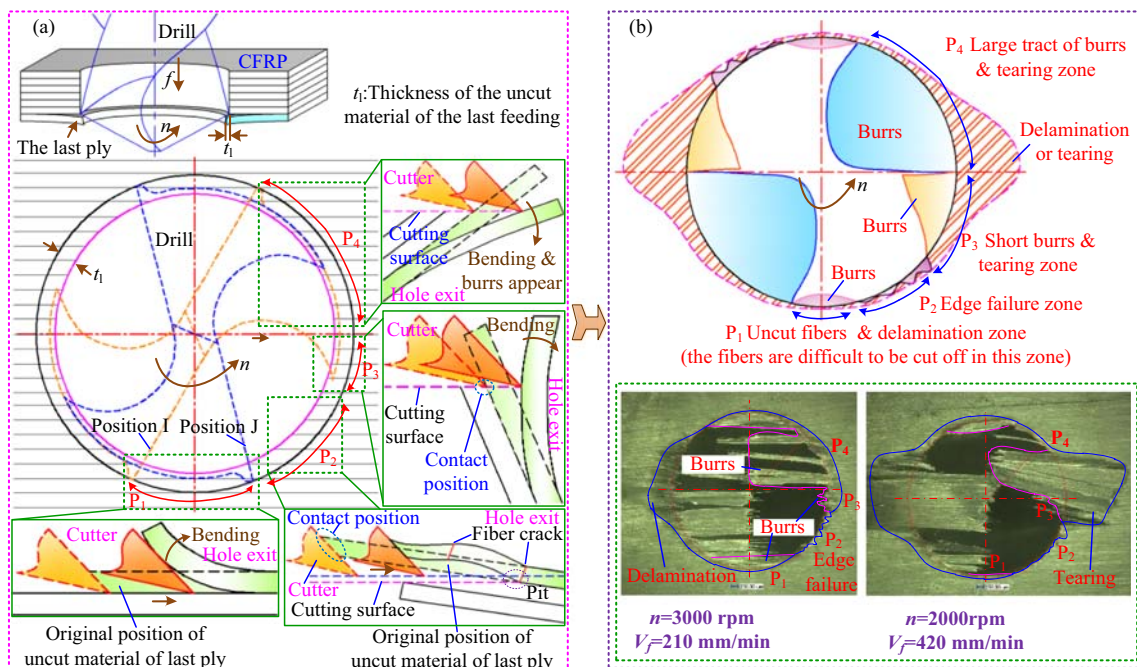


Fig. 10 Cutting states and formation of the burrs

Accordingly, the burrs appear in four fundamental types corresponding to this four cutting states above, as presented in Fig. 10b. The burrs can be classified as (1) in region P_1 , the uncut fiber bundle is accompanied by minor delamination (uncut fibers and delamination zone); (2) In region P_2 , the fibers can be removed, but the saw teeth topography is mapped on the hole edge due to the final breakpoints which are below the cutting surface (edge failure zone); (3) In region P_3 , the contact point between the fibers and the main cutting edges moves toward the nose of the main cutting edge, and the angle between the fiber axis and the cutting direction is still larger than 90 degrees. The cutting or squeezing by the main cutting edge can be terminated until the fibers are bent from the rake face toward the flank face, implying that the bending angle of the fibers is also large. In this process, the fibers are likely to be fractured owing the large bending angle. Of course, the fibers may well evade the cutting edge during this bending. According to experimental observation, some short burrs are prone to form in this region, simultaneously accompanied by the delamination even the tearing (short burrs and tearing zone); (4) In region P_4 , the fibers cannot be removed due to the fibers are easy to evade the cutting edge, and the interlaminar crack is also prone to occur. Thus, large areas of the long burrs accompanied by the tearing appear in this region (large tract of burrs and tearing zone).

Over all, the formation of the burrs can be directly influenced by the cutting states, and there are four states during the drilling of main cutting edges. Then, the burrs appeared in four fundamental types corresponding to this four cutting states, and these states can be classified as uncut fibers and delamination zone, edge failure zone, short burrs and tearing zone, and large tract of burrs and tearing zone, respectively.

5 Conclusions

Exit damages such as burrs and delamination are some of the crucial quality issues in CFRP drilling. In this paper, a novel analytical model is established based on the Winkler elastic foundation beam theory and the cohesive zone model to better understand the mechanism of drill-induced exit-delamination formation. Additionally, according to experimental observation, the formation mechanism of the drill-induced burrs is also analyzed. Then, both of the formation mechanisms of the delamination and the burrs have been investigated. Some key conclusions are drawn from the results presented in this research as follows:

- (1) The critical thrust forces vary regularly as θ changes and reach the maximum when $\theta = 0^\circ/180^\circ$, and reach the second largest value when $\theta = 90^\circ/270^\circ$. The critical thrust force simply reflects the vulnerability of the crack, but

cannot determine the size of the crack. If the critical thrust force is larger, the crack occurs easier.

- (2) The w_{cmax} value determines the size of the crack. The delaminations reach the maximum when $\theta = 0^\circ/180^\circ$ owing to the smallest w_{max} and w_{cmax} , and reach the minimum when $\theta = 90^\circ/270^\circ$ because of the largest w_{max} and w_{cmax} . Therefore, in fact, the most straightforward and effective method is to control the axial displacement of the last ply materials.
- (3) The shape factor K_S decreases with the increasing of feed speed, implying that the effect of the fiber orientation on the delamination is more obvious, and the effect of the spindle speed on the shape factor K_S is not obvious.
- (4) The burrs appear in four fundamental types corresponding to this four cutting states, and these states can be classified as uncut fibers and delamination zone, edge failure zone, short burrs and tearing zone, and large tract of burrs and tearing zone, respectively.

Funding information This study received funding from the National Science Foundation of China (No. 51805164).

References

1. Choudhury MR, Srinivas MS, Debnath K (2018) Experimental investigations on drilling of lignocellulosic fiber reinforced composite laminates. *J Manuf Process* 34:51–61
2. Zhu Z, Guo K, Sun J, Li J, Liu Y, Zheng Y, Chen L (2018) Evaluation of novel tool geometries in dry drilling aluminium 2024-T351/titanium Ti6Al4V stack. *J Mater Process Technol* 259: 270–281
3. Wang X, Shen X, Zeng C, Sun F (2018) Combined influences of tool shape and as-deposited diamond film on cutting performance of drills for CFRP machining. *Surf Coat Technol* 347:390–397
4. Loja MAR, Alves MSF, Bragança IMF, Rosa RSB, Barbosa ICJ, Barbosa JI (2018) An assessment of thermally influenced and delamination-induced regions by composites drilling. *Compos Struct* 202:413–423
5. Xu J, Li C, Mi S, An Q, Chen M (2018) Study of drilling-induced defects for CFRP composites using new criteria. *Compos Struct* 201:1076–1087
6. Deng H, Xu Z (2019) Dressing methods of superabrasive grinding wheels: a review. *J Manuf Process* 45:46–69
7. Çelik A, Lazoglu I, Kara A, Kara F (2015) Investigation on the performance of SiAlON ceramic drills on aerospace grade CFRP composites. *J Mater Process Technol* 223:39–47
8. Su F, Zheng L, Sun FJ, Wang ZH, Deng ZH, Qiu XY (2018) Novel drill bit based on the step-control scheme for reducing the CFRP delamination. *J Mater Process Technol* 262:157–167
9. Feito N, Díaz-Álvarez A, Cantero JL, Rodríguez-Millán M, Miguelez H (2015) Experimental analysis of special tool geometries when drilling woven and multidirectional CFRPs. *J Reinf Plast Compos* 19(19):1215–1220
10. Rahme P, Landon Y, Lachaud F, Piquet R, Lagarrigue P (2015) Delamination-free drilling of thick composite materials. *Compos Part A* 72:148–159
11. Saoudi J, Zitoun R, Gururaja S, Mezlini S, Hajjaji AA (2016) Prediction of critical thrust force for exit-ply delamination during

- drilling composite laminates: thermo-mechanical analysis. *Int J Mach Mach Mater* 18:77–98
12. Ismail SO, Ojo SO, Dhakal HN (2017) Thermo-mechanical modelling of FRP cross-ply composite laminates drilling: delamination damage analysis. *Compos Part B Eng* 108:45–52
 13. Saoudi J, Zitoune R, Gururaja S, Mezlini S, Hajjaji AA (2016) Critical thrust force predictions during drilling: analytical modeling and X-ray tomography quantification. *Compos Struct* 153:886–894
 14. Ojo SO, Ismail SO, Paggi M, Dhakal HN (2017) A new analytical critical thrust force model for delamination analysis of laminated composites during drilling operation. *Compos Part B Eng* 124:207–217
 15. Girot F, Dau F, Gutiérrez-Orrantia ME (2017) New analytical model for delamination of CFRP during drilling. *J Mater Process Technol* 240:332–343
 16. Kim GW, Kang YL, Kim GW (2005) Critical thrust force at propagation of delamination zone due to drilling of FRP/metallic strips. *Compos Struct* 69(2):137–141
 17. Jia Z, Fu R, Niu B, Qian B, Bai Y (2016) Novel drill structure for damage reduction in drilling CFRP composites. *Int J Mach Tools Manuf* 110:55–65
 18. Turki Y, Habak M, Velasco R, Vantomme P (2017) Highlighting cutting mechanisms encountered in carbon/epoxy composite drilling using orthogonal cutting. *Int J Adv Manuf Technol* 3:1–13
 19. Colligan K, Ramulu M (1991) Delamination in surface plies of graphite/epoxy caused by the edge trimming process. *Process Manuf Compos Mater* 49(27):113–125
 20. Sheikh-Ahmad J, Urban N, Cheraghi H (2012) Machining damage in edge trimming of CFRP. *Mater Manuf Process* 27(7):802–808
 21. Hintze W, Brüggemann F (2018) Influence of spatial tool inclination on delamination when milling CFRP. *J Mater Process Technol* 252: 830–837
 22. Hintze W, Hartmann D (2013) Modeling of delamination during milling of unidirectional CFRP. *Procedia CIRP* 8:444–449
 23. Zhou JW, Chen Y, Fu YC, Xu J, Hu A, Liu S (2015) Influence of fiber cutting angle on the machining defects during slotting of CFRP. *J Harbin Inst Technol* 47(7):110–116
 24. Voss R, Seeholzer L, Kuster F, Wegener K (2017) Influence of fibre orientation, tool geometry and process parameters on surface quality in milling of CFRP. *CIRP J Manuf Sci Technol* 18:75–91
 25. Islam F, Ramkumar J, Milani AS (2016) A simplified damage prediction framework for milling of unidirectional carbon fiber-reinforced plastics. *Adv Manuf Polym Compos Sci* 1(4):175–184
 26. Fu R (2017) Reaearch of key technologies for low-damage drilling CFRP composites. Liaoning: Dalian, Dalian University of Technology (In English)
 27. Andoh PY, Davis F, Antonio J (2011) Prediction of a delamination area during drilling of carbon composite laminates structures. *J Sci Technol* 31(2):120–134
 28. Jin PJ, Kim GW, Kang YL (2005) Critical thrust force at delamination propagation during drilling of angle-ply laminates. *Compos Struct* 68(4):391–397
 29. Bao Y (2010) The formation mechanism of disfigurements during drilling and the high-efficiency techniques of drilling C/E composite. Liaoning: Dalian, Dalian University of Technology (In English)
 30. Su F, Zheng L, Sun F, Deng Z, Qiu X (2019) Theoretical modeling for the exit-delamination morphology of the unidirectional CFRPs. *Int J Adv Manuf Technol* 102:533–544
 31. Li H, Qin X, He G, Price MA, Jin Y, Sun D (2017) An energy based force prediction method for UD-CFRP orthogonal machining. *Compos Struct* 159:34–43
 32. Liu WX, Zhou GM, Wang XF, Gao J (2014) Theoretical analysis of crack propagation in composite DCB specimens. *Acta Mater Composit Sin* 31(1):207–212
 33. Fei S, Deng Z, Sun F, Li S, Wu Q, Jiang X (2019) Comparative analyses of damages formation mechanisms for novel drills based on a new drill-induced damages analytical model. *J Mater Process Technol* 271:111–125
 34. Lachaud F, Piquet R, Collombet F, Surcin L (2001) Drilling of composite structures. *Compos Struct* 52(3):511–516
 35. Zitoune R, Collombet F (2007) Numerical prediction of the thrust force responsible of delamination during the drilling of the long-fibre composite structures. *Compos Part A* 38(3):858–866
 36. Voss R, Seeholzer L, Kuster F, Wegener K (2019) Analytical force model for orthogonal machining of unidirectional carbon fiber reinforced polymers (CFRP) as a function of the fiber orientation. *J Mater Process Technol* 263:440–469
 37. Feng P, Wang J, Zhang J, Zheng J (2017) Drilling induced tearing defects in rotary ultrasonic machining of C/SiC composites. *Ceram Int* 43(1):791–799

Publisher's note Springer Nature remains neutral with regard to jurisdictional claims in published maps and institutional affiliations.